Service life estimation of cracked concrete using EIS technique

R. Vedalakshmi
CSIR-Central Electrochemical Research Institute,
Karaikudi-630 006, email : corrveda@yahoo.co.in

Concrete cracking poses a major threat to durability and service life of concrete structures. In the present study estimation of service life of cracked concrete using Electrochemical Impedance Spectroscopy (EIS) technique has been explored. EIS is a powerful tool for measuring the dielectric properties of materials and interfaces. It is fast and allows in-situ, non-destructive and continuous measurements. Uncracked and cracked cylindrical concrete specimens were exposed under marine atmosphere prevailing at Mandapam as shown in Fig.1. EIS measurements were carried out periodically using conventional three electrodes arrangement. Diffusion coefficient of chloride (D_{eff}) in cm^2/s and corrosion current (I_{corr}) were determined from the high and low frequency of the EIS plot as shown in Fig.2.

Determination of time to initiation of corrosion, T_i

From the Nyquist plot, the resistance of the concrete (R_c) was determined from the high frequency arc. Using the Nernst-Einstein equation, the diffusion coefficient of chloride was calculated.

$$D_{eff} = \frac{R\,T\,a}{F^2\,C_{cl}^{-}\,R_c} \qquad (1)$$

Where a - Cell constant (t/A), R_c - Resistance from the high frequency EIS spectra, R- Gas constant, T – Temperature, C_{cl}^- - Chloride ion concentration and F is the Faraday Constant. After determining the D_{eff} using the eqn. (1), time to initiate corrosion was calculated using the following formula:

$$T_i = \frac{x^2}{4\,D_{eff}\,erf^{-}\left(1-\frac{C_x}{C_s}\right)^2} \qquad (2)$$

where T_i - time for chloride ions to reach C_x (x, t) at cover depth x, x-cover of concrete, cm, C_s- surface chloride concentration, % by weight of cement, C_x- threshold chloride concentration at which corrosion is initiated on the rebar, % by weight of cement. The results are tabulated in Table1.

Determination of time to propagation, T_p

The charge transfer resistance of the rebar (R_{ct}) was determined from the low frequency region of the Nyquist plot and substituted in Stern- Geary equation to obtain I_{corr}. Time to cracking (T_{cr}) was calculated using Maaddawy model as per the following equation.

$$T_{cr} = \left[\frac{7117.5\left(D+2\delta_0\right)\left(1+\gamma+\psi\right)}{i\,E_{cf}}\right]\left[\frac{2Cf_{ct}}{D}+\frac{2\delta_0 E_{cf}}{(1+\gamma+\psi)(D+2\delta_0)}\right] \qquad (3)$$

Anyone who stops learning is old, whether twenty or eighty. Anyone who keeps learning stays young. The greatest thing you can do it to keep your mind young- *Mark twain*

where D - diameter of the rebar, C- cover thickness, i_{corr} - corrosion current density, µA/cm^2 E_{cf}- effective elastic modulus of concrete that is equal to $\frac{E_c}{(1+\phi_{cr})}$, E_c- elastic modulus of concrete, $E_c = 5000\sqrt{f_{ck}}$ (I.S 456:2000), Φ_{cr}- concrete creep coefficient assumed as 2.35 as per CSA standard (CSA, 1994), γ- Poisson's ratio of concrete assumed as 0.18 as per CSA, δ_0- porous layer assumed to be of 10 µm thickness, f_{ct}- tensile strength of concrete, (as per IS 456: 2000), f_{ck} - compressive strength of concrete at the end of 365 days.

The advantage of this model over other models is that the concrete properties such as creep coefficient of concrete, Poisson's ratio, elastic modulus of concrete, compressive and tensile strength of concrete are included in the equation. The results are tabulated in Table 2.

Results and Discussion

The average crack widths measured on 15 and 25 mm cover concrete were 0.14 and 0.22 mm respectively. The RH and temperature prevailing at Mandapam were monitored over a period of two years and the average values were found to be 76 and 30°C respectively. Comparison of the Nyquist plot of the rebar embedded in uncracked concrete with that of cracked concrete after an exposure period of 635 days under marine atmospheric condition, is given in Fig. 2. It was noted that the diameter of the high frequency arc of rebar in cracked concrete was lower than that of uncracked concrete, which indicated that the rates of diffusion of chloride and moisture were higher in cracked concrete. The low frequency tail showed that rebar was under diffusion controlled process in both the concretes and confirmed that rust had not initiated even for low cover of 15 mm. From this observation, it was inferred that the depth of the crack was not extended upto the cover of 15 mm.

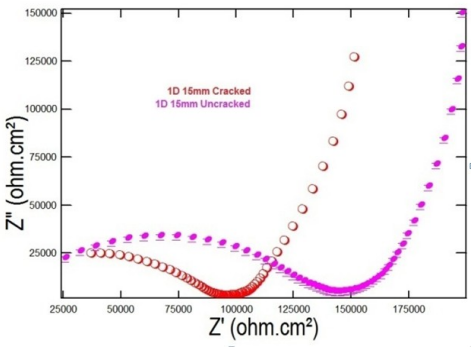

Fig.2: Nyquist plot of rebar embedded in uncracked/cracked concrete

Fig.1. Specimens exposed at corrosion testing center, Mandapam

Ambition is the last refuge of the failure- *Oscar Wilde*

The D_{eff} values of cracked and uncracked concrete were compared (Table 2), which showed that D_{eff} was two-times higher for the former than that for the latter. The values of T_i and T_{cr} for cracked and uncracked concrete for both cover thicknesses have been compared in Table 1 and 2. It was clearly evident that the service life was 6 years for 15 mm cover in cracked concrete and reduced the service life of uncracked concrete by 1/5 times. When the cover of concrete was increased from 15 mm to 25 mm, the service life in cracked concrete increased only 2 times that of 15 mm cover concrete; however, in uncracked concrete, the service life was found to be 7.5 times that of 15 mm cover concrete. From the foregoing discussion, it was concluded that the presence of cracks in concrete exposed to marine atmospheric conditions caused premature failure of concrete and probability of occurrence of cracks was more when the cover concrete thickness was lower.

Table.1. Determination of D_{eff} and T_i

Cover/flow of chloride	Resistance, Ω-cm^2				$D_{eff,1.75}$, m^2/s	T_i, days
	March-'11	July-'11	Oct.-'11	June-'12		
Uncracked						
15 mm	20.6 x 10^3	44.87X10^3	130 x 10^3	99 x 10^3	4.47 x 10^{-11}	2410
25 mm	35.05 x 10^3	48.55X10^3	86.45 x 10^3	199 x 10^3	4.62 x 10^{-11}	6690
				Average	4.55 x 10^{-11}	
Cracked						
15 mm			3.26 x 10^4	---------	1.07 x 10^{-10}	1020
25 mm			5.5 x 10^4		8.00 x 10^{-11}	2850

Table.2 Prediction of time to cracking

Cover (mm)	Chloride, %	R_{ct}, Ω-cm^2		i_{corr}, µA/cm^2		Time to cracking (T_p), days	$T_i + T_p$, years
		Initial	After 630 days	Initial	After 630 days		
Uncracked-15	0	740 x 10^3	1110 x 10^3	0.0473	0.032	8537	30
Cracked	0	740 x 10^3	151 x 10^3	0.0473	0.232	1177	6
Uncracked-25	0	2710 x 10^3	7320 x 10^3	0.0129	0.0047	75382	225
Cracked	0	2710 x 10^3	130 x 10^3	0.0129	0.269	1340	11.5

Conclusions

1. When the cover of the uncracked concrete was increased to 25 from 15 mm, the service life increased to 225 years from 39 years.
2. The presence of cracks reduced the service life by 1/5 times that of uncracked concrete when concrete cover was 15 mm thick. It nullified the effect of direction of cover of concrete.

The probability of occurrence of premature failure of cracked concrete under marine atmospheric condition was more for concrete having lower cover thickness.

References

Maaddawy and Khaled Soudki, Cement & Concrete Composites 29 (2007), pp. 168-175.

Diagnostics of Microbiologically Influenced Corrosion in Cooling Water Systems

R. P. George and U. Kamachi Mudali
Corrosion Science and Technology Group (CSTG), IGCAR
Kalpakkam (TN) - 603 102: email: rani@igcar.gov.in

Dramatic changes in the climate due to green house emissions and escalating costs of energy are forcing to take all steps to conserve energy. In this context, effectiveness of cooling water systems employed in various power plants to maintain highest electrical energy output per tonne of fuel is particularly important. Despite efforts to provide efficient design of heat exchangers and effective maintenance during operation, fouling and corrosion under the influence of microbes pose a big threat to this objective. All the common natural resources of cooling water like, rivers, lakes and seawater provide enough microbial fauna that will colonize various material surfaces in cooling water systems. These microbes secrete slime, trap nutrients and multiply, resulting in a complex biofilm, which degrades the properties of the condenser materials, the process being termed as "biofouling." Microbial fouling layer up to about a few μm thickness, made up of microbes and their metabolic products, builds up within hours of exposure of materials to aquatic media. This forms the base for subsequent build up of several centimeters thick macrofouling biomass essentially composed of macroalgae, barnacles, mussels etc. This type of growth inside the pipelines restricts the flow thereby, diagnosing the biological role in the corrosion process is very intricate. Even isolation of corrosion causing microorganisms from a specific environment does not adequately argument to exclusively state that certain microbes are responsible for the corrosion failure. The task of identifying MIC is multidisciplinary and needs an integrated approach. Chemical and microbiological analysis, material surface characterization and corrosion product analysis may help us to identify the role of microbes. However, only corrosion process simulation can identify the mechanism and thereby confirm the true role of microbes. In this article, two metal-microbe interactions that commonly occur in cooling water systems are presented.

Carbon Steel Corrosion by Iron Oxidizing Bacteria

The condenser cooling water system of the Fast Breeder Test Reactor (FBTR) at Kalpakkam was commissioned in 1985 and after 5 years, heavy tuberculation and thinning of walls of carbon steel (CS) pipes resulted in replacement of several small diameter pipes (Fig.1). Several studies have indicated association of Iron Oxidising Bacteria (IOB) with CS tuberculation. However, a

systematic study was carried out to simulate CS tuberculation under different conditions of flow parameters, dissolved oxygen (DO) concentration and density of IOB. Attempts were also made to distinguish the specific role of microbes in establishing the corrosion process from normal electrochemical corrosion by detailed deposit analysis. Tubercles were initiated under aerated static raw water conditions with an IOB density of 1.2 x 10^2cfu/cm^2, but they did not grow further. Well developed tubercles were formed (Fig. 2) in raw water studies with flow rate of (3- 120 L/h), saturated oxygen concentration of 6- 8 ppm and IOB density ranging from 2.8 x 10^4 cfu/cm^2 to 3.2 x 10^4cfu/cm^2; average corrosion rate of specimens was found to be high (11.8 ± 0.3 mpy). Correlation between corrosion rates and various parameters like DO, Total Viable Count (TVC) in water and in biofilm, showed that significant correlation existed only between corrosion rate and TVC of bacteria in biofilms.

IOB derive energy from the oxidation of Fe^{2+} to Fe^{3+}. Since the reaction $Fe^{2+} \rightarrow Fe^{3+} + e^-$ yields very little energy (11.3 kcal/g-atom), large quantities of ferrous ions must be processed and this capacity of IOBs makes them a potential hazard in cooling water systems using fresh water with CS materials. XRD analysis of CS corrosion products showed that, in the presence of IOB, poorly crystalline ferrihydrite formed with weak and broad lines at d-spacing of 1.97 and 1.72 A° due to rapid oxidation of Fe(II) by IOB and poorly ordered ferrihydrite aggregates readily initiating nodule formation for tuberculation. IOBs associated with

Fig.1 Heavy tuberculation and thinning of wall of FBTR

Fig.2 Stereomicrograph of CS coupon with (a)growing tubercles and (b) tubercles that has stopped growing after 3 month exposure to flowing water

nodules scavenge oxygen for respiration and hence the region inside nodules are free of oxygen compared to outside. Thus, the principle role of IOBs is to form an efficient oxygen concentration cell by assisting nodule formation. Analysis of the particle size and charge of the CS corrosion products in the presence of IOB gave further bacterial signatures like smaller particle size (< 1µm) and higher negative charge compared to sterile systems.

Crevice Corrosion of Stainless Steel in Cooling Water Systems

Stainless steels (SS) of basic 18Cr-8Ni composition are commonly used in nuclear

power plants in high purity environments such as reactor coolant systems, emergency systems, reactor auxiliary systems such as plate-and-frame exchangers, heat exchanger tubing, impellers and housing and as heat exchanger shells. The highly corrosion resistant passive film of SS can breakdown under the influence of inorganic and organic acids and chloride environments; biofilms can precipitate at the metal/biofilm interface under such environments. A detailed study was undertaken by forming different biofilms; mixed biofilms of algae and bacteria formed in open reservoir conditions (Fig.3), pure bacterial and algal biofilms formed in laboratory pure cultures and examining their effect on the electrochemical characteristics of SS and corrosion initiation. Detailed biochemical characterization of the mixed biofilms developed over a period of 123 days on 304 SS by exposing in open reservoir, showed higher values of diatom count, (276 cells cm^{-2}), particulate organic carbon (9.4 µg cm^{-2}) and chlorophyll content (0.16 µg cm^{-2}), thereby proving algal domination in the mixed biofilm. However, total bacterial density was also high in normal biofilms (2 x 10^5 cfu cm^{-2}). From this biofilm, constituent microbial species like *Pseudomonas* sp. (aerobic bacteria), *Desulfovibrio* sp. (anaerobic bacteria) and photosynthetic algae like *Coelastrum* sp. and *Oscillatoria* sp. were isolated and cultured and 304 SS specimens were immersed in these pure cultures for the formation of respective biofilms. Electrochemical potentiodynamic anodic polarization studies were carried out to compare 304 SS specimens covered with natural mixed biofilms and biofilms formed from pure culture of algae and bacteria independently. The parameters of interest were open circuit potential (OCP), passive current density (i_p), breakdown potential (E_b) and repassivation potential (E_{repass}). As the mixed biofilm developed on the 304 SS specimen, the OCP became nobler (shifted to noble direction from -180 mV(SCE) to -150 mV(SCE)), breakdown potential also showed ennoblement and passive current density decreased because biofilm acted as a physical barrier to diffusion of ions from the metal to the environment. As the thickness and age of the normal biofilm (dominated by algae) increased with increase in the duration of exposure in reservoir water, passive current increased and the specimen covered with biofilm formed over 123 days showed two orders increase in the passive current density (i_p). SEM photomicrograph of this surface on removal of biofilm revealed crevice corrosion initiation (Fig.4). Among the pure culture biofilms, algal biofilms showed ennoblement as algal photosynthesis can increase the kinetics of cathodic oxygen reduction, $O_2 + 2H_2O + 4e^- \rightarrow 4OH^-$, and this increase may shift the corrosion potential of the metal/alloy to the noble direction. However, pure culture biofilms of aerobic and anaerobic bacteria and photosynthetic algae by themselves did not show any effect on passive current density. This clearly confirmed that a consortium of algae and bacteria in normal biofilms influenced the crevice corrosion behaviour of SS. The predominantly algal-dominated

regions on the specimen surface, where oxygen concentration increases due to algal photosynthesis, OCP ennoblement created a good cathode whereas bacterial respiration under bacterial colonies formed active anodic areas due to oxygen depletion. This cathode-anode creation was responsible for the crevice corrosion initiation. It can also be assumed that biofilms have much lower ionic resistance than a conventional crevice as it can permit rapid propagation of localized corrosion even at low chloride environments.

Thus, the detailed study of these two metal-microbe interactions demonstrated that uncovering MIC - based failures in technological equipment requires an independent approach in each case. This also exemplifies that confirmation of microbial influence in each type of corrosion environment is possible only by simulation of the corrosion parameters found in the field which have a direct effect on the process.

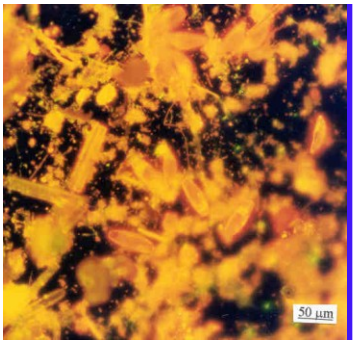

Fig. 3 Epifluorescence micrograph of biofilm on 304 SS exposed to reservoir water

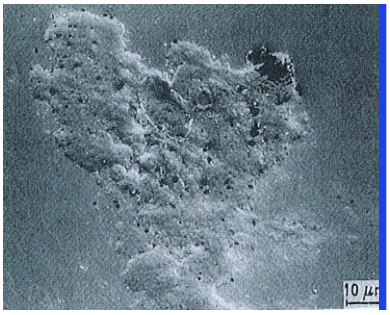

Fig. 4 Scanning electron micrograph showing crevice corrosion attack on 304 SS specimen after the biofilm was removed

Cross word on failure analysis terminologies

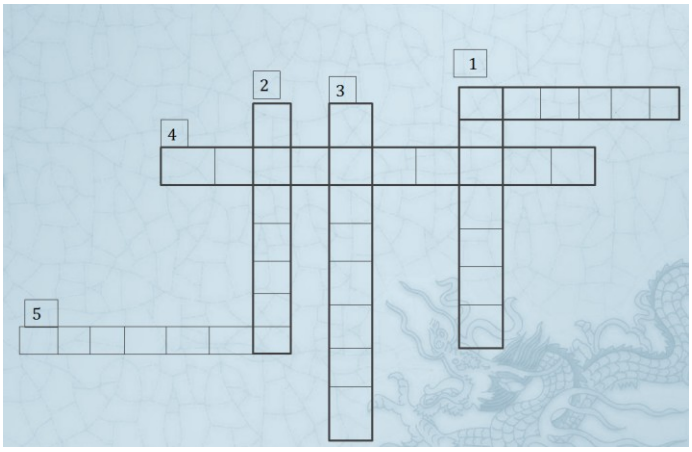

Across:

1) LG used soft mud from refining for packing material [6]
4) Add little tungsten on reheating so as to get alloy steel with rust adherence [10]
5) Handling with a dredge may spoil the material over time [7]

Down:

1) U may resize it but still it may stick up [7]
2) I pave a layer on stainless steel which made it corrosion resistant [7]
3) LiH in Mecca is considered a corrosive one [8]